Energy Conversion and Management 89 (2015) 339–348

Contents lists available at ScienceDirect

Energy Conversion and Management

journal homepage: www.elsevier.com/locate/enconman

Study on the matching performance of a low temperature reverse Brayton air refrigerator

Yu Hou, Shanju Yang, Xingya Chen, Shuangtao Chen, Tianwei Lai *

State Key Laboratory of Multiphase Flow in Power Engineering, Xi'an Jiaotong University, Xi'an 710049, PR China

ARTICLE INFO

Article history:
Received 12 August 2014
Accepted 30 September 2014

Keywords:
Reverse Brayton cycle
Refrigerator
Turboexpander
Bump foil bearing
Matching
Thermal performance

ABSTRACT

A small reverse Brayton cycle air refrigerator was designed and fabricated. Bump-type air journal foil bearing, pressurized thrust gas bearing and centrifugal blower as brake were employed in the turboexpander. Usually, constant brake inlet pressure is set in a reverse Brayton refrigerator. However, the unchanged brake inlet pressure cannot adapt to the changing temperature and expansion ratio during the cooling down process, which could go against the system performance. In this article, the relationship between the turboexpander operation parameters and brake pressure was disclosed through theoretical analysis. The performance curve was analyzed through numerical simulation using CFX. A matching model was established based on the theoretical analysis and numerical simulation. Brake pressure feedback control was then proposed and applied in the experimental study. Thermal performance of the refrigerator was tested under varied operating conditions (different expansion ratios, temperatures and brake pressures). The results indicated that the appropriate brake pressure facilitated system good thermal performance under both design and off-design conditions, and the theoretical results agreed well with the experimental data.

1. Introduction

Due to advantages of small size, light weight, high operating reliability, long life, wide range of refrigeration temperature, environmental friendly, reverse Brayton refrigerator has been widely used in space applications [1], high altitude and space environment simulator [2], aircraft and road air-conditioning system [3,4], high temperature superconducting [5,6], natural gas and hydrogen plant [7–9]. Especially, the application of gas bearing has brought reverse Brayton refrigerator the extraordinary advantages of high speed operation, completely oil-free, less energy-consuming, environmental suitability, etc. [10–15].

So far, much research has been focused on reverse Brayton refrigerator. James and Razanib [16] carried out theoretical analysis of the thermodynamic optimization of reverse Brayton cycles with different configurations. Bromberg et al. [17] developed simple models to investigate the optimization of a turbo-Brayton cycles for cooling current leads. Nicholas et al. [1] described a reverse turbo-Brayton cycle cooler employing gas bearing for the Hubble Space Telescope. Chang et al. [5] presented a thermodynamic design of Brayton refrigerator for sub-cooling liquid nitrogen from 72.0 K to 65.0 K. Hirai et al. [6] designed a Neon turbo-Brayton cycle refrigerator for HTS power machines and they developed a turbo-compressor to control the cooling power. Zhao et al. [13] studied the compact heat exchanger and turboexpander of elastic support foil bearing by experiment. Guo and Huai [18] carried out optimization design of the heat exchanger in an irreversible regenerative Brayton cycle. Besaratia et al. [19] presented a simultaneous optimization study of a combined Brayton and inverse Brayton cycles. Hou et al. [20] used turboexpander in a compression refrigeration system for air condition and made it more efficient than a conventional cycle. Whereas, quite a small amount of investigation for matching characteristic between expansion wheel and brake blower are available, which are of the same significance.

In this article, the thermal performance of the turboexpander, especially, the influences of the brake pressure on the system thermal efficiency were studied theoretically and experimentally. Theoretical results on the matching performance of expansion wheel and brake blower were obtained. And, with brake pressure feedback control, the experiments were carried out with varied operation parameters which were adjusted by changing the brake inlet pressure. In the experiment, the turboexpander (shaft diameter is 12.00 mm) rotating speed were located in the range of 150–215 krpm. This study aims to present matching and braking characteristics of the turboexpander and its influence on the refrigerator.

* Corresponding author. Tel.: +86 29 82664921.
E-mail address: laitianwei@mail.xjtu.edu.cn (T. Lai).

http://dx.doi.org/10.1016/j.enconman.2014.09.078
0196-8904/

Nomenclature

A_{min}	area of nozzle throat (m^2)
c_s	isentropic spouting velocity ($m\ s^{-1}$)
D	diameter (m)
h	real isentropic enthalpy drop of turboexpander ($J\ kg^{-1}$)
hs	ideal isentropic enthalpy drop of turboexpander ($J\ kg^{-1}$)
h_{th}	the specific energy ($J\ kg^{-1}$)
k_T	air adiabatic exponent
n	rotating speed ($r\ min^{-1}$)
n_d	design speed of the blower ($r\ min^{-1}$)
n_Z	polytropic exponent in nozzle
p	pressure (Pa)
P	power (W)
q_{mT}	mass flow rate of expansion gas ($kg\ s^{-1}$)
Q_0	cooling capacity (W)
Q_d	design inlet volume flow rate of the blower ($m^3\ min^{-1}$)
Q_{0F}	inlet volume flow rate of blower ($m^3\ min^{-1}$)
R	gas constant of air ($J\ kg^{-1}\ K^{-1}$)
T	temperature (K)
u_1	expansion wheel inlet peripheral velocity ($m\ s^{-1}$)
Z	compression factor

Greek

ε_T	expansion ratio
η_s	ideal isentropic efficiency of the turboexpander
ρ	density ($kg\ m^{-3}$)
μ	slip factor
β	friction and windage loss factor

Subscripts

s	ideal isentropic
$0T$	inlet of the turboexpander
$1T$	inlet of the wheel
$2T$	outlet of the turboexpander
$0F$	inlet of the blower
$2F$	outlet of the blower

2. Theoretical analysis

Turboexpander is the core component in a reverse Brayton air refrigerator. The cooling capacity Q_0 and the efficiency of turboexpander η_s are defined as [21]:

$$Q_0 = q_{mT} h_s \eta_s \tag{1}$$

$$\eta_s = \frac{h}{h_s} = \frac{h_{0T} - h_{2T}}{h_s} \tag{2}$$

where h_{0T} is the inlet enthalpy of the turboexpander ($J\ kg^{-1}$), h_{2T} is the outlet enthalpy of the turboexpander ($J\ kg^{-1}$).

It can be seen from Eq. (1) that, a certain amount of cool capacity can be obtained through the cooperation of three factors. Whereas, the increase of ideal isentropic enthalpy drop h_s and mass flow rate q_{mT} will increase cost of the system directly, and adjustment of the mass flow rate is usually achieved through complicated structural measures. Therefore, great attentions should be first paid to the improvement of the turboexpander efficiency.

There are too many factors that affect the efficiency of the turboexpander, for instance, velocity factor, blade angle, reaction degree and characteristic ratio, of which, characteristic ratio is essential. Characteristic ratio is the ratio of inlet peripheral speed of expansion wheel to ideal isentropic velocity of turboexpander. The isentropic enthalpy drop h_s and the characteristics ratio u_1/c_s can be described as [21]:

$$h_s = \frac{k_T}{k_T - 1} R T_{0T} \left(1 - \varepsilon_T^{\frac{k_T - 1}{k_T}}\right) \tag{3}$$

$$\frac{u_1}{c_s} = \frac{\pi D_{1T} n}{60\sqrt{2h_s}} = \frac{\pi D_{1T}}{60\sqrt{2\frac{k_T}{k_T - 1} R\left(1 - \varepsilon_T^{\frac{1-k_T}{k_T}}\right)}} \frac{n}{\sqrt{T_{0T}}} \tag{4}$$

where T_{0T} is the inlet temperature of the turboexpander (K), and D_{1T} is the inlet diameter of the expansion wheel (m).

In order to obtain high expansion efficiency, characteristics ratio should be maintained in a certain range [21]. As shown in Eq. (4), the variation of characteristics ratio will take place with the change of expansion ratio, inlet temperature of turboexpander and rotating speed. During the cooling down process of the refrigerator, inlet temperature of the turboexpander will continue to decrease before get to a stable state [2]. Since the interaction between the expansion wheel and brake blower is very complex, the key for the optimum characteristic ratios is that the rotating speed which is not only important for the expansion wheel, but also for the brake blower should be settled to adapt this variation.

At stable state, the brake power P_F was about 99% of the output power of the impeller P_T.

$$P_F = 0.99 P_T \tag{5}$$

where P_F is the brake power of the blower (W), and P_T is the output power of the wheel (W).

The mass flow rate of the turboexpander can be described as below [21]:

$$q_{mT} = \frac{A_{min} p_{0T}}{\sqrt{Z_{0T} R T_{0T}}} \sqrt{\frac{k_T (n_Z - 1)}{k_T - 1} \left(\frac{2}{n_Z + 1}\right)^{\frac{n_Z + 1}{n_Z - 1}}} \tag{6}$$

where p_{0T} is the inlet pressure of the turboexpander (Pa), and Z_{0T} is the compression factor at inlet of the turboexpander.

Differing Eq. (1), then the output power of the turboexpander P_T can be calculated as:

$$\begin{aligned} P_T &= \frac{k_T}{k_T - 1} R T_{0T} \left(1 - \varepsilon_T^{\frac{1-k_T}{k_T}}\right) q_{mT} \eta_s \\ &= A_{min} p_{0T} \left(\frac{k_T}{k_T - 1}\right)^{1.5} \left(1 - \varepsilon_T^{\frac{1-k_T}{k_T}}\right) \left[\frac{R(n_Z - 1)}{Z_0} \left(\frac{2}{n_Z + 1}\right)^{\frac{n_Z + 1}{n_Z - 1}}\right]^{0.5} \eta_T T_{0T}^{0.5} \end{aligned} \tag{7}$$

It is clear that the output power P_T is linearly related to $T_{0T}^{0.5}$ under constant isentropic efficiency, constant inlet and outlet pressure of turboexpander.

As the blower is of axial admission, the specific energy h_{th} transmitted to the air is assessed with the Euler equation [22]:

$$h_{th} = \mu u_{2F}^2 = \mu \left(\frac{\pi D_{2F} n}{60}\right)^2 \tag{8}$$

where u_{2F} is the outlet circumferential speed of the blower ($m\ s^{-1}$), and D_{2F} is the outlet diameter of the blower (m).

The inlet volume flow rate Q_{0F} is determined by rotating speed approximately [22]:

$$Q_{0F} = Q_d \frac{n}{n_d} \tag{9}$$

As shown in Eq. (9), volume of the suction gas is linearly related to the rotating speed. From Eqs. (4), (8) and (9), the brake power is obtained:

$$P_F = (1+\beta)h_{th}Q_{0F}\rho_{0F} = \frac{60(1+\beta)\mu Q_d R^{1.5} D_{2F}^2 (u_1/c_s)^3}{\pi n_d D_{1T}^3}\left[\frac{2k_T}{k_T-1}\left(1-\varepsilon_T^{\frac{1-k_T}{k_T}}\right)\right]^{1.5}\rho_{0F}T_{0T}^{1.5} \quad (10)$$

where ρ_{0F} is the inlet density of the blower (kg m^{-3}), and T_{0F} is the inlet temperature of the blower (K).

It can be inferred from Eqs. (7) and (10) that, in order to get the persistent efficiency during the cooling down process, a relation between the brake pressure and the operation parameters of the turboexpander must also be satisfied:

$$p_{0F}T_{0T} = \frac{\pi p_{0T}A_{min}n_d D_{1T}^3}{169.7(1+\beta)\mu Q_d D_{2F}^2 (u_1/c_s)^3}\left[\frac{n_z-1}{Z_{0T}}\left(\frac{2}{n_z+1}\right)^{\frac{n_z+1}{(n_z-1)}}\Big/\left(1-\varepsilon_T^{\frac{1-k_T}{k_T}}\right)\right]^{0.5}\eta_T T_{0F} \quad (11)$$

where p_{0F} is the inlet pressure of the blower (Pa).

And a relation between the rotating speed and the operation parameters of the turboexpander might be:

$$n = 84.8\frac{k_T R(u_1/c_s)}{\pi D_{1T}(k_T-1)}\left(1-\varepsilon_T^{\frac{1-k_T}{k_T}}\right)^{0.5}T_{0T}^{0.5} \quad (12)$$

From the discussions above, we know that the essential factor of getting the matching performance is to obtain the performance curve of the turboexpander. Simulations on the turboexpander were carried out for this purpose.

3. Test apparatus description

As shown in Fig. 1(a), the test rig is composed of three parts: the air supply section, the refrigeration section and the blower section. The air supply section consists of an air filter, a screw compressor, a freezing dryer, two molecular sieves and a buffer. It can provide 600.0 N m^3 h compressed air at 1.30 MPa. The refrigeration section is composed of an electric proportional valve, a precision filter, the turboexpander and a high vacuum cold box which includes a plate-fin heat exchanger. The blower section contains the centrifugal blower, a fan, an electric proportional valve and a throttling valve. The two molecular sieves work alternately to reject the residual liquid particles (water and oil) after the freezing dryer. The vacuum degree of the $\phi 0.7 \times 2.0$ m stainless steel cold box can reach 5.0E−5 Pa. The cold side of the turboexpander is placed verticality in the vacuum cold box. The main parameters of the turboexpander and the system are listed in Table 1. As shown in Fig. 1 (b), the thermodynamic process of the cycle is illustrated in the *T-s* diagram. As shown in Fig. 1(b), 1–2 is the compression process of the compressor, 2–3 is the isobaric cooling process, 3–4 is the precooling process in the heat regenerator, 4–5 is the expansion process of the turboexpander, and 5–6 is the heat recovery process in the heat regenerator.

The gas in the tank is absorbed by the centrifugal blower and then filled into the tank after compression. The heat from the compression process is rejected by heat leak along the pipe and the fan in the blower section. Therefore, the inlet temperature of the blower could be kept equal to the ambient temperature. The electric proportional valve together with the throttling valve is collocated, which could keep the pressure of the gas in the tank on certain values. The schematic view and photograph of the turbo-rotor system are shown in Fig. 2. The rotor is supported by two bump foil journal bearings and two aerostatic thrust bearings. For guaranteeing the operation stability of the turboexpander, structure form and parameters of bump air foil bearing were carefully designed and tested. The details of the bump foil air bearing are

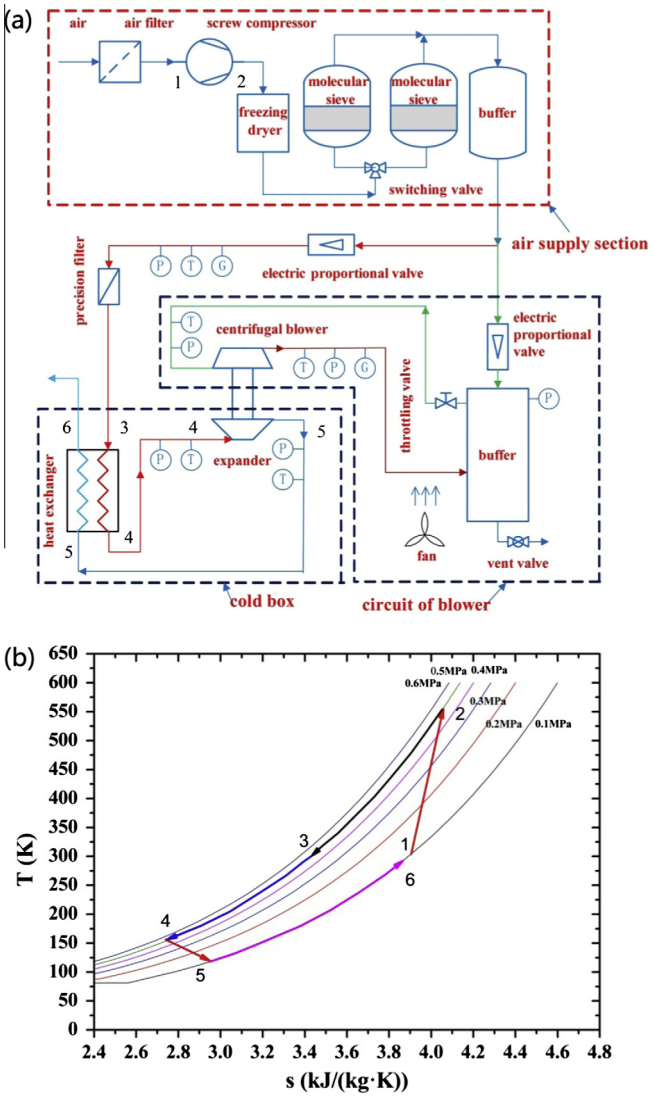

Fig. 1. The reverse Brayton refrigerator (a) test rig; (b) *T-s* diagram of the reverse Brayton cycle.

described in Table 1. The bump foil and top foil were fixed by means of screw and spacer (see Fig. 2(b) and (c)). The experimental results indicated that both good assembly performance and low costs can be achieved through the presented configuration.

All the platinum resistance thermometers have been calibrated by Chinese Academy of Sciences, and the maximum uncertainty is ±0.2 K in the temperature range of 320.0–80.0 K. The full scale uncertainty of the pressure gauge is ±0.5% in the pressure range of 0–1.000 MPa. The 4 mm diameter eddy current sensors with linearity <±2% and static resolution of 0.1 μm were used to monitor the rotor speed. The uncertainty of the rotating speed is ±1 rpm. The full scale uncertainty of the flow rate is ±1.5% in the range of 300–6000 N L/min. According to Moffat method [23], the uncertainty analysis of the efficiency, characteristic ratio and cooling capacity are performed and the calculated results were 0.2%, 0.2% and 1.5% respectively.

4. Discussion

4.1. Numerical simulation of expansion process

With the purpose of obtaining the theoretical performance curve, a numerical simulation on the turboexpander was

Table 1
Main design parameters of the turboexpander and the gas bearing.

Items	Value	Items	Value
Main design parameters of the turboexpander		*Main design parameters of the gas bearing*	
Inlet pressure	0.500 MPa (abs.)	Foil thickness	50 μm
Outlet pressure	0.110 MPa (abs.)	Bearing length	12.00 mm
Inlet temperature	139.0 K	Bump height	0.40 mm
Flow rate	95.0 N m^3 h	Number of bumps	19
Isentropic efficiency	57.8%	Journal diameter	12.93 mm
Characteristic ratio	0.670	Journal length	13.00 mm
Expansion wheel diameter	24.00 mm	Radial clearance	15 μm
Blower diameter	30.00 mm		
Rotor diameter	12.00 mm		
Rotating speed	163.8 krpm		

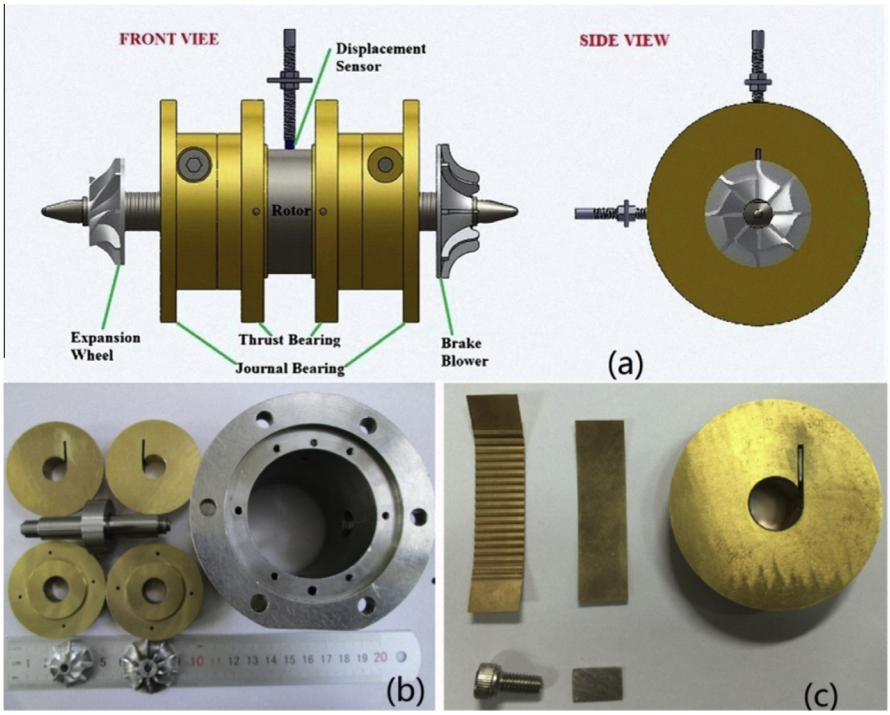

Fig. 2. Schematic view and photograph (a) schematic view of the turboexpander; (b) photograph of the turboexpander; (c) photograph of the bump foil bearing.

performed by CFX and validated by experimental data. The operation parameters of the simulations and the experiments are listed in Table 2. The three-dimensional structured grid was constructed and steady the three-dimensional calculations were conducted. Grid independence tests showed that the grid size of 421,591 nodes and 375,365 elements could satisfy the accuracy. Since the flow condition in diffuser was symmetrical, only one quarter of the physical domain in diffuser was considered and the symmetrical boundary condition is applied. As the flow conditions were the same in each port of the nozzle and impeller, only one port of them was considered and the periodic boundary condition was applied. To acquire results closing to the practical cases, both heat loss and roughness of the wall were considered in the simulation.

Table 2
Operation parameters of simulations and experiments.

Items	Simulation	Experiment
The 1st group		
Inlet pressure of turboexpander	0.400 MPa (abs.)	0.400–0.402 MPa (abs.)
Outlet pressure of turboexpander	0.107 MPa (abs.)	0.107 MPa (abs.)
Inlet temperature of turboexpander	157.0 K	156.3–159.1 K
The 2nd group		
Inlet pressure of turboexpander	0.500 MPa (abs.)	0.497–0.500 MPa (abs.)
Outlet pressure of turboexpander	0.110 MPa (abs.)	0.110 MPa (abs.)
Inlet temperature of turboexpander	139.0 K	138.2–141.1 K
The 3rd group		
Inlet pressure of turboexpander	0.580 MPa (abs.)	0.582–0.584 MPa (abs.)
Outlet pressure of turboexpander	0.113 MPa (abs.)	0.113 MPa (abs.)
Inlet temperature of turboexpander	137.0 K	136.7–139.6 K

Simulation contours at the design point are shown in Fig. 3. There are uniform variations of pressure and temperature in the expansion process. As shown in Fig. 4, the solid lines show the predicted performance curves calculated by the simulations and they agree well with the measured efficiencies. In the 1st group (Fig. 4(a)), the measured maximum efficiency is 60.6% at $u_1/c_s = 0.671$ with the maximum relative error of 3.5%. In the 2nd group (Fig. 4(b)), the measured maximum efficiency is 62.4% at $u_1/c_s = 0.668$ with the maximum relative error of 2.4%. In the 3rd group (Fig. 4(c)), the measured maximum efficiency is 61.4% at $u_1/c_s = 0.668$ with the maximum relative error of 2.7%. The maximum efficiencies are somewhat different under the varied expansion ratios, but the optimal characteristics ratio is around 0.670. Both the measured and the predicted efficiencies in Fig. 4(a) are lower than that in Fig. 4(b) and (c), possibly because the expansion

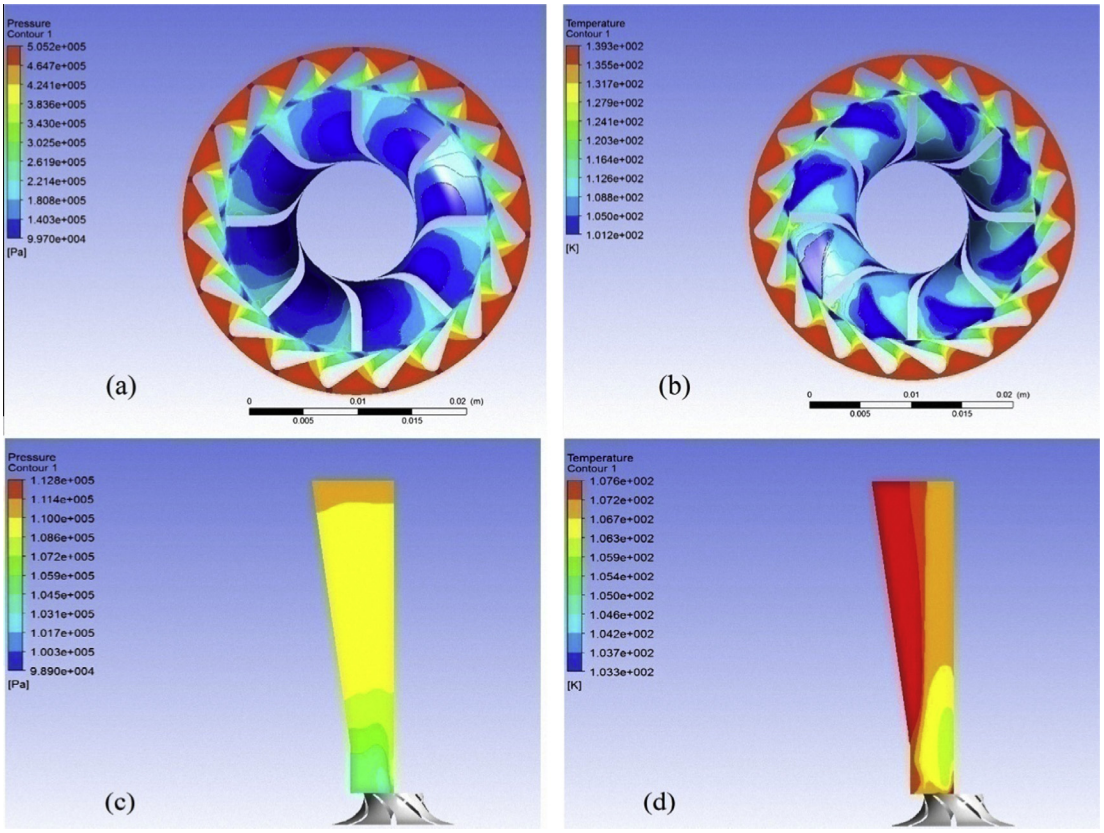

Fig. 3. Contours of the turboexpander (a) pressure in nozzle and expansion wheel; (b) temperature in nozzle and wheel; (c) pressure in diffuser; (d) temperature in diffuser.

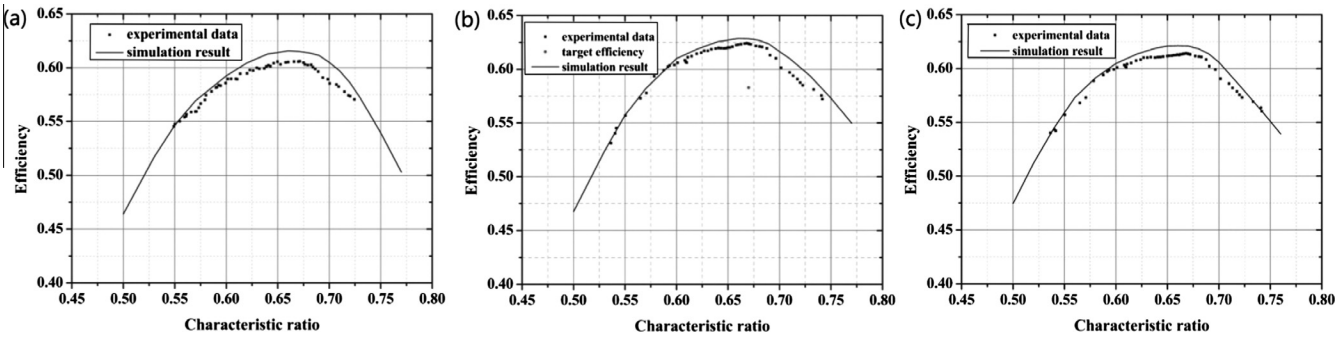

Fig. 4. Performance curves at different expansion ratios (a) $\varepsilon_T = 3.74$; (b) $\varepsilon_T = 4.55$; (c) $\varepsilon_T = 5.13$.

ratio is rather different from the design value. It can be inferred that the numerical simulation can effectively predict the performance curve and therefore provide a basis for the following matching calculation.

4.2. Theoretical calculation on matching performance

In order to investigate the influence of compression process of the brake blower on the performance of the turboexpander, the system matching studies were conducted. Fig. 5 shows the flowchart of the matching analysis. For a given brake pressure, the stable rotating speed, characteristic ratio and efficiency could be got through computation based on the model in Fig. 5. For a given characteristic ratio, the required brake pressure versus operation varied parameters of turboexpander could also be obtained through calculation. The corresponding program was developed via Matlab code.

The calculations were carried out based on the 2nd group in Table 2. As shown in Fig. 6(a), under a given brake pressure, the characteristic ratio increases as the inlet temperature of turboexpander decreases. And the efficiency increases first and then decreases. When the turboexpander is operated at the design inlet temperature 139.0 K, the characteristic ratios increase to 0.729, 0.695, and 0.656 and the corresponding efficiencies are 0.572, 0.599 and 0.611, respectively. As shown in Fig. 6(b), the rotating speed mainly decreases with the decrease of the turboexpander inlet temperature. That is because the lower the turboexpander inlet temperature is responsible for the lower the enthalpy drop. It can be seen from Fig. 6 that a specific brake pressure could only match a particular situation and when the operation parameters of the turboexpander change it will not be the optimal value. Therefore, with a brake pressure applied in the cooling down process, efficiency will always be lower than the maximum or just reach the maximum at some specific point. So a constant brake pressure

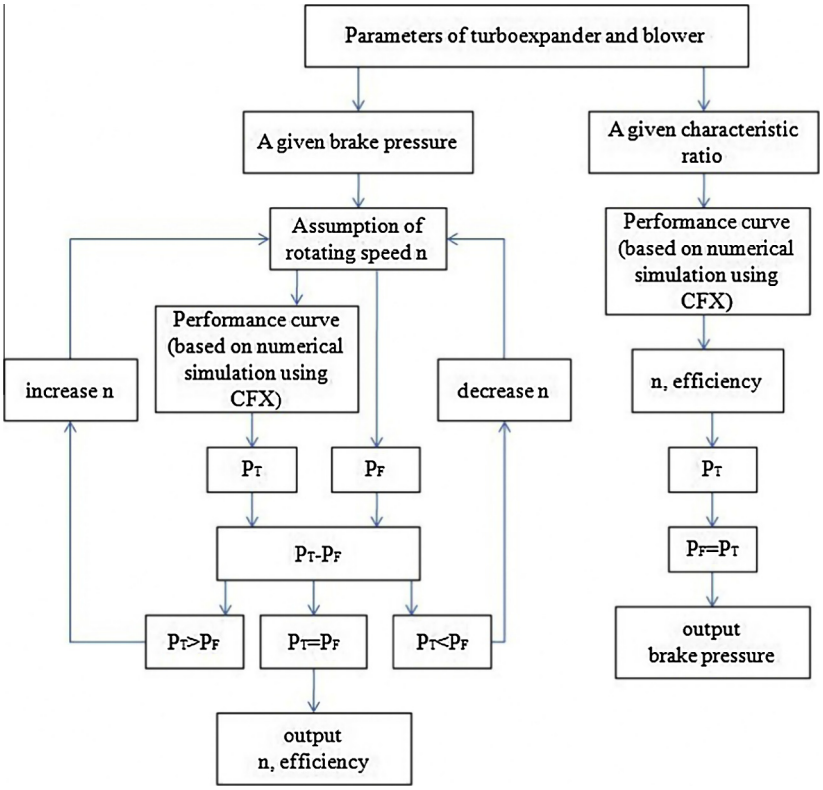

Fig. 5. The flowchart of the matching analysis.

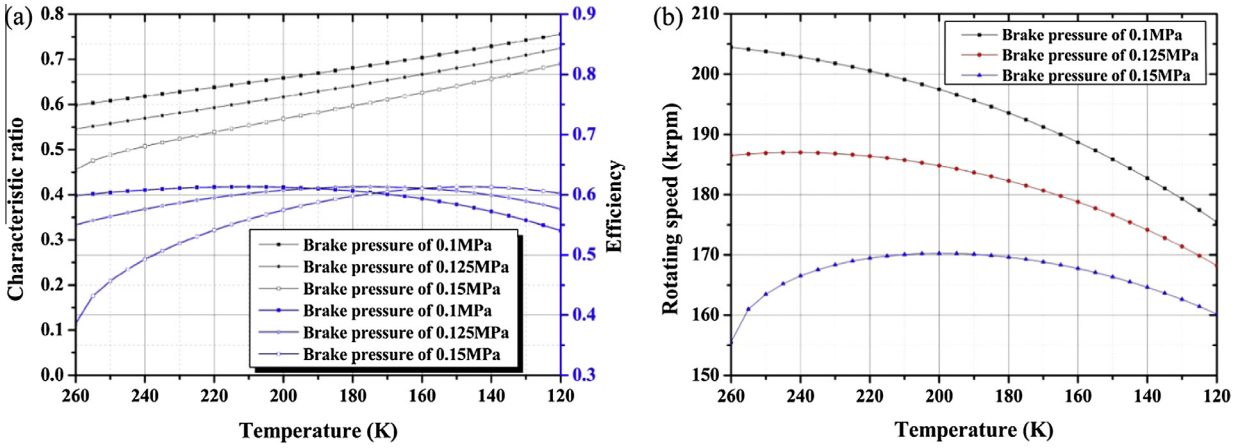

Fig. 6. Theoretical results under constant brake pressure (a) characteristic ratio and efficiency; (b) rotating speed.

is not appropriate in the cooling down process. In addition, sometimes the refrigerator may work under off-design conditions of varied expansion ratio and brake pressure should also be adjusted to an optimal value.

As shown in Fig. 7(a), when the characteristic ratio is settled, the efficiency is fixed accordingly. In order to keep the characteristic ratio constant, the brake pressure increases with the decrease of the inlet temperature of turboexpander. As shown in Fig. 7(b), the brake pressure increases from 0.071 MPa to 0.153 MPa when the inlet temperature decreases from 250.0 K to 120.0 K. The theoretical results in Figs. 6 and 7 indicate that in the cooling down process and the off-design condition the matching of the brake and the expansion process is necessary for the desired optimum efficiency, e.g. for the purpose of high efficiency in both the cooling down process and the off-design condition, the adjustment of the brake pressure is necessary.

4.3. Experimental study on matching performance

In order to investigate the influence of matching performance on system refrigerating performance, a constant brake pressure test and a brake pressure feedback control test were conducted. The operation parameters are listed in Table 3. NI 6251 data acquisition board and the Labview based data acquisition and real-time display program were applied for data process. The brake pressure was adjusted continuously through an electric proportional valve (SMC: ITV3050-214CL) and a throttling valve. The characteristic ratio was kept around 0.670 through the adjustment of brake pressure.

As shown in Fig. 8(a), the cooling down speed of the refrigerator in test 2 is much faster than that of test 1. Within 60 min, the outlet temperature reached 131.5 K and 112.3 K in the two tests, respectively. After 120 min, the outlet temperature of turboexpander is

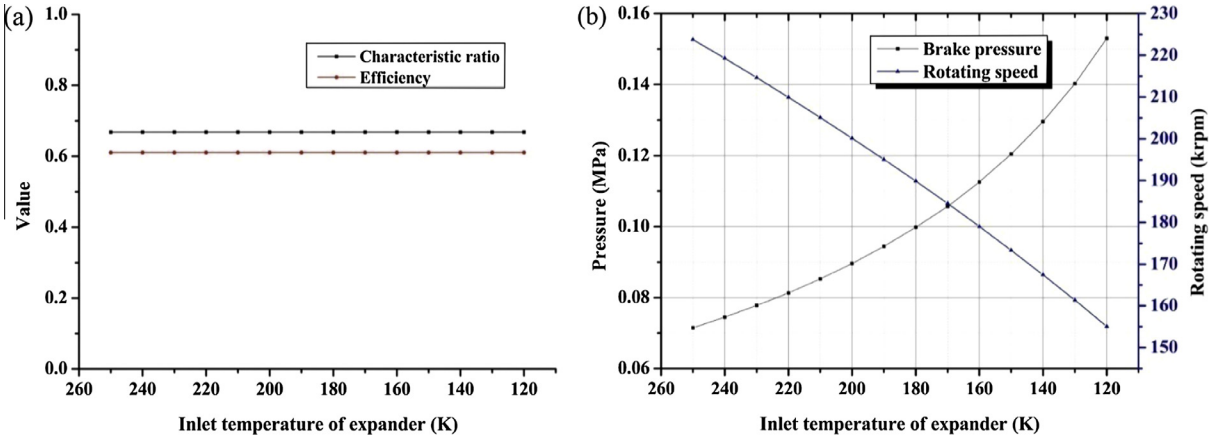

Fig. 7. Theoretical results under constant characteristic ratio (a) characteristic ratio and efficiency; (b) brake pressure and rotating speed.

Table 3
Operation parameters of four tests.

Items	Value	Items	Value
Test 1		*Test 2*	
Inlet pressure of turboexpander	0.497–0.499 MPa (abs.)	Inlet pressure of turboexpander	0.497–0.500 MPa (abs.)
Outlet pressure of turboexpander	0.110 MPa (abs.)	Outlet pressure of turboexpander	0.109–0.110 MPa (abs.)
Inlet temperature of blower	306.2–309.7 K	Inlet temperature of blower	301.1–305 K
Brake pressure	0.100–0.103 MPa (abs.)	Brake pressure	Feedback control
Test 3		*Test 4*	
Inlet pressure of turboexpander	0.399–0.402 MPa (abs.)	Inlet pressure of turboexpander	0.581–0.586 MPa (abs.)
Outlet pressure of turboexpander	0.107 MPa (abs.)	Outlet pressure of turboexpander	0.113 MPa (abs.)
Inlet temperature of blower	303.1–307.6 K	Inlet temperature of blower	304.5–308.3 K
Brake pressure	Feedback control	Brake pressure	Feedback control

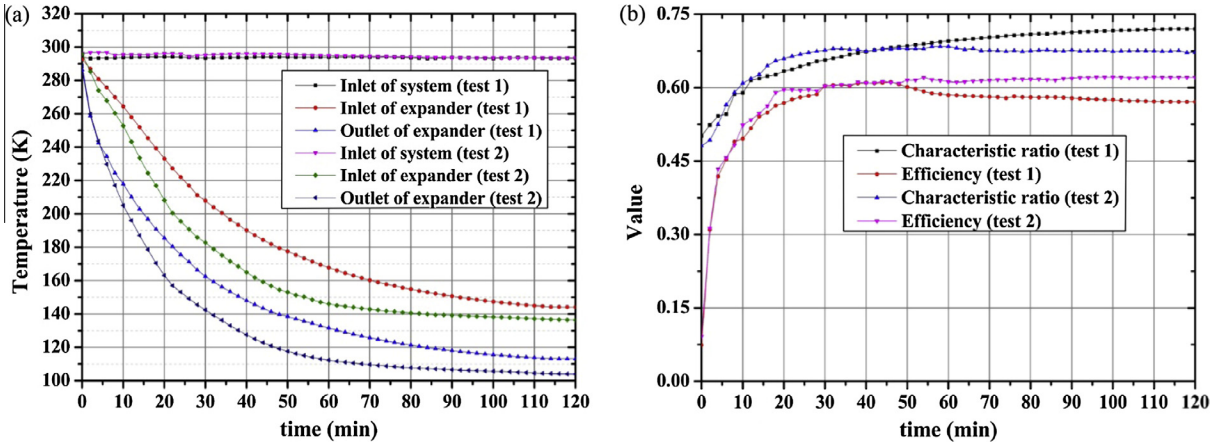

Fig. 8. Comparison between tests 1 and 2 (a) cooling down process; (b) efficiency and characteristic ratio.

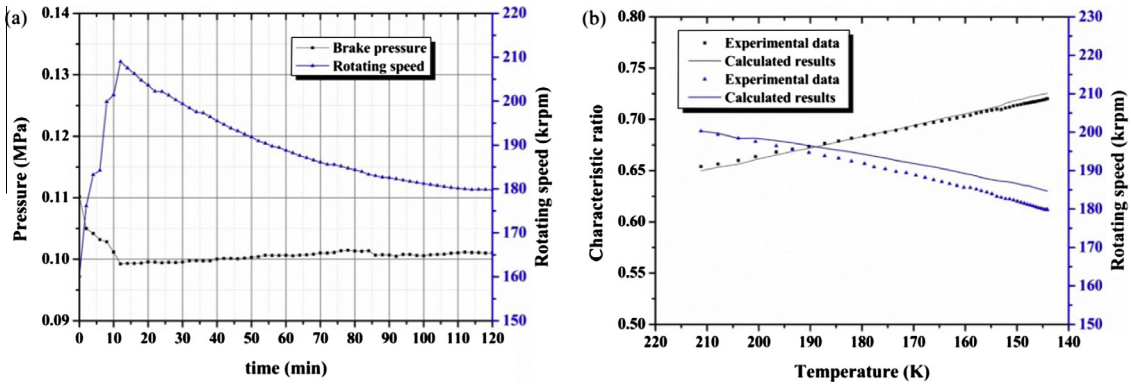

Fig. 9. Matching performance in test 1 (a) brake pressure and rotating speed; (b) comparisons between experimental and calculated results.

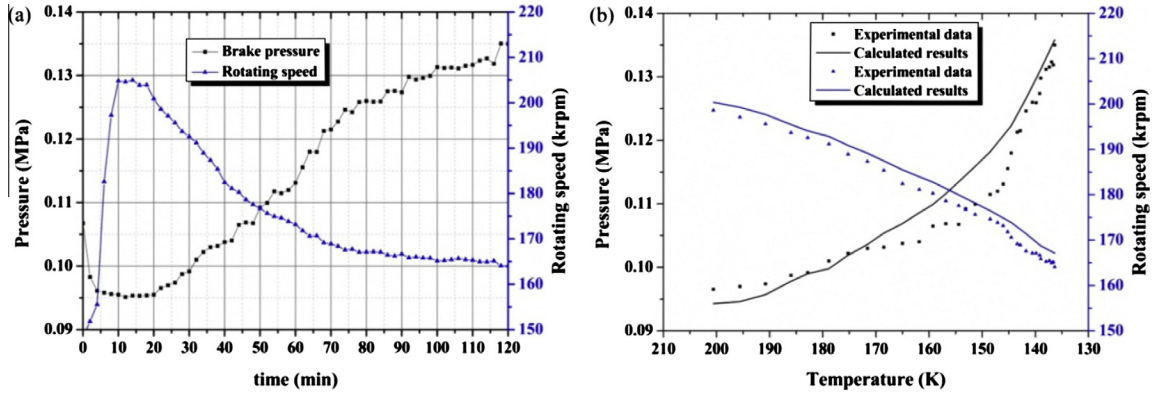

Fig. 10. Matching performance in test 2 (a) brake pressure and rotating speed; (b) comparisons between experimental and calculated results.

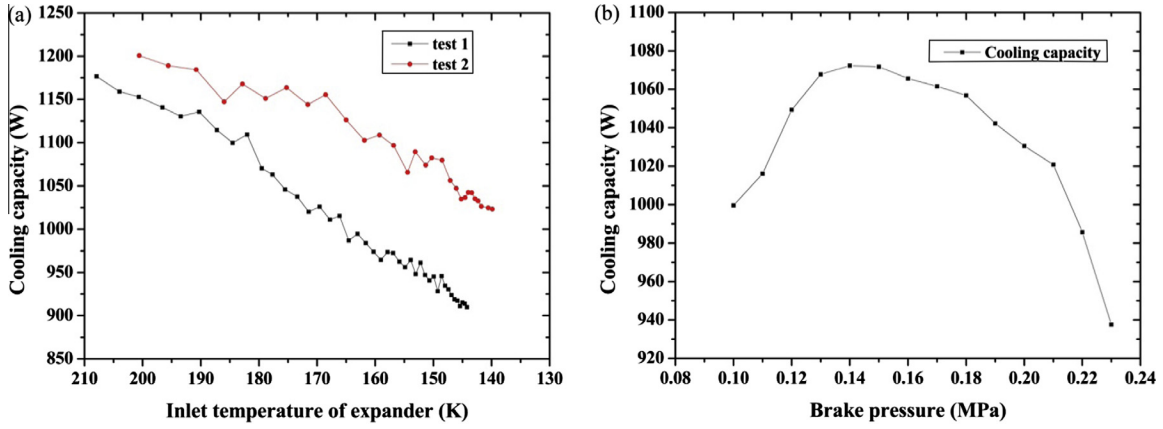

Fig. 11. Cooling capacity (a) variations with turboexpander inlet temperature; (b) variations with brake pressure.

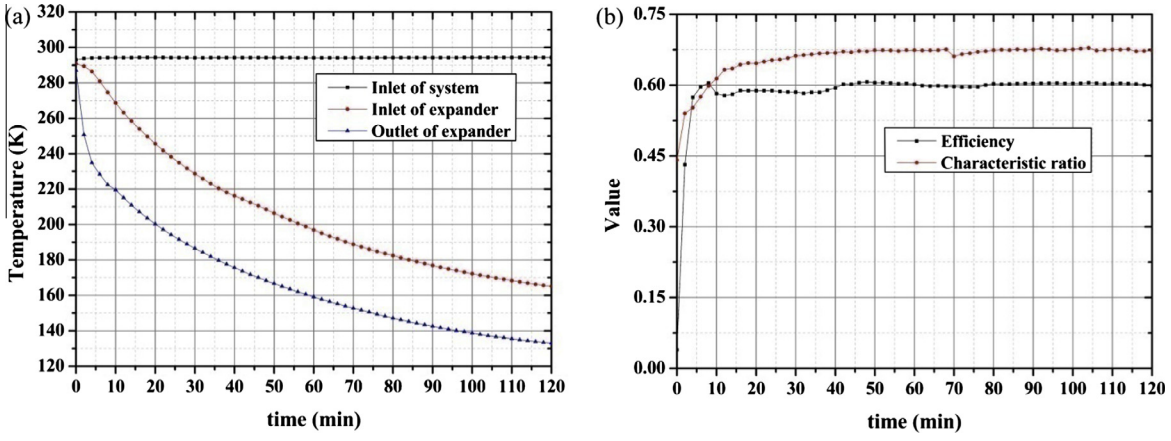

Fig. 12. Refrigeration performance in test 3 (a) cooling down process; (b) efficiency and characteristic ratio.

stabilized in 113.1 K in test 1 while it is stabilized in 103.9 K in test 2. The reason can be explained in Fig. 8(b), the characteristic ratios in test 2 were adjusted closely to the optimum value. The efficiency in test 1 is lower in most of the time and the final efficiency is 0.571. In test 2, the efficiency is kept high in almost all the time and the stable efficiency is 0.621. As shown in Fig. 10, to keep the characteristics ratio closing to the optimum value, the brake pressure was raised from 0.096 MPa to 0.135 MPa at the temperature range of 200.6–136.4 K. The theoretical results and the experimental data agreed well with each other in Figs. 9(b) and 10(b), and the relations described in Eqs. (11) and (12) were also validated. The characteristics ratio increase linearly from 0.650 to 0.725 when the inlet temperature decreases from 211.2 K to 144.1 K in the cooling down process in test 1 (see Fig. 9(b)). While the characteristic ratios from 200.6 K to 136.4 K in test 2 keep nearly the same to the optimum value (see Fig. 8(b)) through the adjustment of the brake inlet pressure. Obviously, under constant inlet parameters of system and expansion ratio of turboexpander,

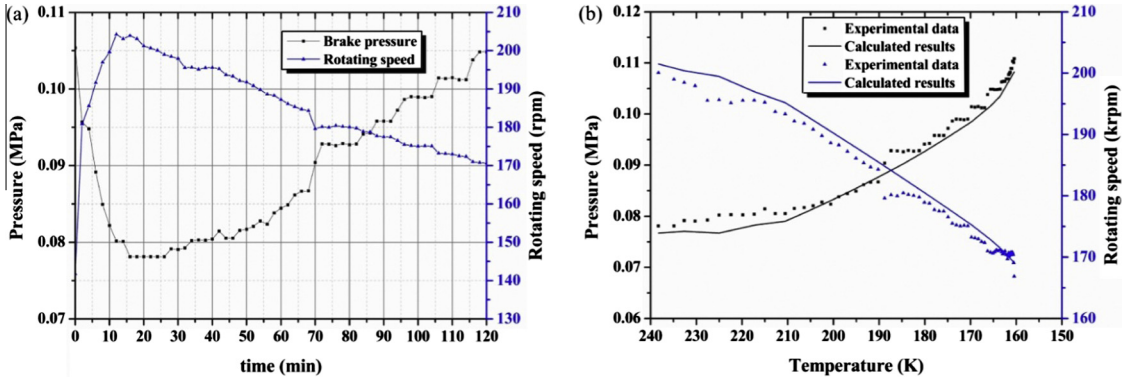

Fig. 13. Matching performance in test 3 (a) brake pressure and rotating speed; (b) comparisons between experimental and calculated results.

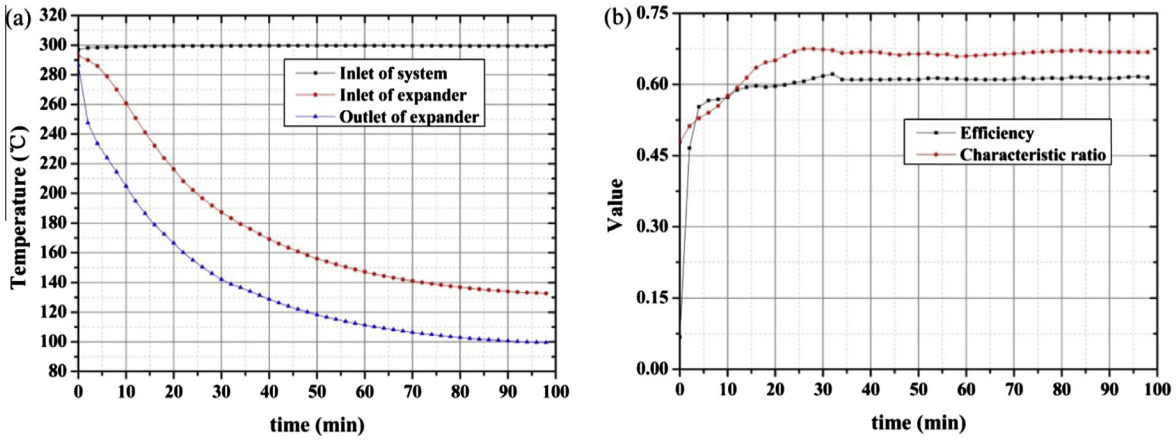

Fig. 14. Refrigeration performance in test 4 (a) cooling down process; (b) efficiency and characteristic ratio.

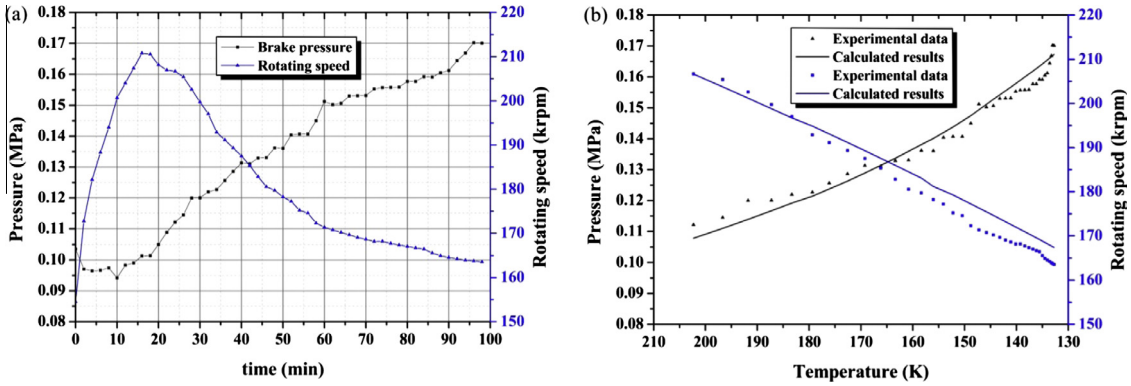

Fig. 15. Matching performance in test 4 (a) brake pressure and rotating speed; (b) comparisons between experimental and calculated results.

the increase of the characteristics ratio is usually caused by lower brake power. To achieve high system efficiency, the corresponding brake pressure feedback control is necessary.

The cooling capacity of the turboexpander is shown in Fig. 11(a). The cooling capacity decreases with the decrease of the inlet temperature. Comparing the two tests, the cooling capacity in test 2 is larger than that of test 1. The difference is 127 W at 144.1 K which is the lowest inlet temperature of test 1. The reason can be found in Fig. 8(b), the efficiencies in test 2 were larger with brake pressure feedback control. As shown in Fig. 11(b), the variations of cooling capacity with brake pressure were presented. The turboexpander inlet temperature was in the range of 138.2–141.1 K, meanwhile, the inlet and outlet pressure of the turboexpander are listed in Table 3 test 1. The cooling capacity of the turboexpander will decrease with the relative lager and smaller brake pressure. To improve the system efficiency, an appropriate brake pressure and the brake pressure feedback control are quite necessary.

The studies of system off-design performance with brake pressure feedback control were also conducted in tests 3 and 4. The expansion ratio in test 3 is smaller than the designed value, and is larger than the designed value in test 4. The operation parameters of the two tests are also described in Table 3.

As shown in Fig. 12, the outlet temperature of turboexpander reaches 133.1 K within 120 min in test 3. As shown in Fig. 14, the outlet temperature of turboexpander reaches 99.6 K within

98 min in test 4. In test 3 the brake pressure was raised from 0.078 MPa to 0.111 MPa in the temperature range of 238.3–160.4 K (see Fig. 13), while in test 4, the brake pressure was raised from 0.108 MPa to 0.167 MPa in the temperature range of 202.3–132.7 K (see Fig. 15). After all, the 60.3% system efficiency of test 3 in Fig. 12(b) and the 61.4% system efficiency of test 4 in Fig. 14(b) shows that with brake feedback control, the refrigerator can still achieve good performance under off-design conditions. The possible matching of the brake pressure and the expansion process was achieved with the brake pressure feedback control under off-design conditions.

5. Conclusion

In this article the thermal performance of the turboexpander, matching performance of the brake blower and expansion wheel, cooling down performance of the refrigerator were investigated under varied operation conditions. The relationship between the operation parameters of the turboexpander and brake pressure was disclosed through detailed theoretical analysis. To get the persistent high efficiency during the cooling down process, the inverse proportional relationship between the brake pressure and inlet temperature of turboexpander must be satisfied, which can also provide the basis for matching analysis of cryogenic turboexpander. Brake pressure feedback control makes possible the matching of different working conditions, and the minimum free-load refrigerating temperature of 99.6 K was reached within 98 min. The refrigerator had good thermal performance under both design and off-design conditions, and the theoretical results agreed well with the experimental data. Due to the good performance of the bump foil bearings, the test apparatus operated stably in a wide rotating speed range within various operating conditions.

Acknowledgements

This project was supported by the National Nature Science Foundation of China (51306135), the Specialized Research Fund for the Doctoral Program of Higher Education (20130201110038) and the Fundamental Research Funds for the Central Universities.

References

[1] Nicholas Jedrich, Darell Zimbelman, Walter Swift and Francis Dolan. A mechanical cryogenic cooler for the Hubble Space Telescope. Presented at the 39th Space Congress, FL, USA; 2002.
[2] Hou Y, Zhao HL, Chen CZ, Xiong LY. Development in reverse Brayton refrigerator in China. Cryogenics 2006;46:403–7.
[3] Spence Stephen WT, John Doran W, Artt David W. Design, construction and testing of an air-cycle refrigeration system for road transport. Int J Refrig 2004;27(5):503–10.
[4] Zhao Hongli, Hou Y, Zhu Yongfeng, Chen Liang, Chen Shuangtao. Experimental study on the performance of an aircraft environmental control system. Appl Therm Eng 2009;29:3284–8.
[5] Chang Ho-Myung, Park CW, Yang HS, Sohn Song Ho, Lim Ji Hyun, Oh SR, et al. Thermodynamic design of 10 KW Brayton refrigerator for HTS cable. AIP Conf Proc 2012;1434:1664–71.
[6] Hiraia H, Suzukia Y, Hirokawaa M, Kobayashia H, Kamiokaa Y, Iwakuma M, et al. Development of a turbine refrigerator for high temperature superconductor applications. Physica C 2009;469:1857–61.
[7] Najjar Yousef SH, Zaamout Mahmoud S. Cryogenic power conversion with regasification of LNG in a gas turbine plant. Energy Convers Manage 1993;34(4):273–80.
[8] Kostowski Wojciech J, Usón Sergio. Comparative evaluation of a natural gas expansion plant integrated with an IC engine and an organic Rankine cycle. Energy Convers Manage 2013;75:509–16.
[9] Ohlig Klaus, Bischoff Stefan. Dynamic gas bearing turbine technology in hydrogen plants. Adv Cryog Eng 2012;57:814–9.
[10] Eber N, Quack H, Schmid C. Gas bearing turbines with dynamic gas bearings and their application in helium refrigerators. Cryogenics 1978;18(11):585–8.
[11] Molyneaux AK, Leonhard M. The use of spiral groove gas bearings in a 350,000 rpm cryogenic expander. Tribology 1989;32(2):197–204.
[12] Kato T, Miyake A, Kawano K, Hamada K, Hiyama T, Iwamoto S, et al. Design and test of a wet type helium turbo-expander with an alternator as a brake. Adv Cryog Eng 1994;39:917–24.
[13] Zhao Hongli, Hou Yu, Chen Liang. Experimental study on a small Brayton air refrigerator under 120 °C. Appl Therm Eng 2009;29:1702–6.
[14] Ghosh Subrata K, Sahoo Ranjit K, Sarangi Sunil K. Experimental performance study of cryogenic turbo turboexpander by using aerodynamic thrust bearing. Appl Therm Eng 2010;30:1304–11.
[15] Ghosh Subrata, Mukherjee Parboti, Sarangi Sunil. Development of bearings for a small high speed cryogenic turboexpander. Ind Lubr Tribol 2010;6(1):3–10.
[16] Streita James, Razanib Arsalan. Thermodynamic optimization of reverse Brayton cycles of different configurations for cryogenic applications. Int J Refrig 2013;36(5):1529–44.
[17] Bromberg L, Michael Philip, Minervini JV, Dietz Anthony. Evaluation of turbo-brayton cycle for cooling current leads: integrated current lead/heat exchanger. AIP Conf Proc 2012;1434:993–1000.
[18] Guo Jiangfeng, Huai Xiulan. Optimization design of heat exchanger in an irreversible regenerative Brayton cycle system. Appl Therm Eng 2013;58(1–2):77–84.
[19] Besarati SM, Atashkari K, Jamali A, Hajilooa A, Nariman-zadeha N. Multi-objective thermodynamic optimization of combined Brayton and inverse Brayton cycles using genetic algorithms. Energy Convers Manage 2010;51:212–7.
[20] Hou Shaobo, Li Huacong, Zhang Hefei. Open air–vapor compression refrigeration system for airconditioning and hot water cooled by cool water. Energy Convers Manage 2007;48:2255–60.
[21] Whitfield A, Baines NC. Design of radial turbomachines. Longman Scientific & Technical; 1990. ISBN 0-470-21667-0.
[22] Cumpsty NA. Compressor aerodynamics. Longman Scientific & Technical; 1989. ISBN 0-470-21334-5.
[23] Moffat Robert J. Describing the uncertainties in experimental results. Exp Therm Fluid Sci 1988;1:3–17.